Cellular and Molecular Life Sciences (2022) 79:27
https://doi.org/10.1007/s00018-021-04022-2

ORIGINAL ARTICLE

Biophysical and biochemical properties of PHGDH revealed by studies on PHGDH inhibitors

Yuping Tan[1] · Xia Zhou[2] · Yanqiu Gong[3] · Kun Gou[2] · Youfu Luo[1] · Da Jia[4] · Lunzhi Dai[3] · Yinglan Zhao[2] · Qingxiang Sun[1]

Received: 3 June 2021 / Revised: 2 November 2021 / Accepted: 3 November 2021 / Published online: 31 December 2021

Abstract

The rate-limiting serine biogenesis enzyme PHGDH is overexpressed in cancers. Both serine withdrawal and genetic/pharmacological inhibition of PHGDH have demonstrated promising tumor-suppressing activities. However, the enzyme properties of PHGDH are not well understood and the discovery of PHGDH inhibitors is still in its infancy. Here, oridonin was identified from a natural product library as a new PHGDH inhibitor. The crystal structure of PHGDH in complex with oridonin revealed a new allosteric site. The binding of oridonin to this site reduced the activity of the enzyme by relocating R54, a residue involved in substrate binding. Mutagenesis studies showed that PHGDH activity was very sensitive to cysteine mutations, especially those in the substrate binding domain. Conjugation of oridonin and other reported covalent PHGDH inhibitors to these sites will therefore inhibit PHGDH. In addition to being inhibited enzymatically, PHGDH can also be inhibited by protein aggregation and proteasome-mediated degradation. Several tested PHGDH cancer mutants showed altered enzymatic activity, which can be explained by protein structure and stability. Overall, the above studies present new biophysical and biochemical insights into PHGDH and may facilitate the future design of PHGDH inhibitors.

Keywords Compound screening · Allosteric inhibition · Nucleotide-binding domain · Protein degradation · Cancer mutation

Introduction

A hallmark of cancer cells is the ability to reprogram their metabolism to promote fast growth and proliferation, and overcome cellular stresses [1]. The serine synthesis pathway is one of the frequently upregulated cancer metabolic pathways [2]. Serine is a vital source of 'one-carbon' units, which are required for the synthesis of cellular building blocks such as proteins, nucleic acids, and lipids [3]. In addition to using exogenous serine, cells synthesize serine through a branch of glycolysis [4]. The rate-limiting step

Yuping Tan, Xia Zhou and Yanqiu Gong have contributed equally.

✉ Lunzhi Dai
lunzhi.dai@scu.edu.cn

✉ Yinglan Zhao
zhaoyinglan@scu.edu.cn

✉ Qingxiang Sun
qingxiang.sun@scu.edu.cn

[1] Department of Pathology, State Key Laboratory of Biotherapy and Cancer Center, West China Hospital, Sichuan University and Collaborative Innovation Center of Biotherapy, Chengdu 610041, China

[2] State Key Laboratory of Biotherapy and Cancer Center, West China Hospital, West China Medical School, Sichuan University, 17#, 3rd Section, Ren min South Road, Chengdu 610041, China

[3] National Clinical Research Center for Geriatrics and Department of General Practice, State Key Laboratory of Biotherapy, West China Hospital, Sichuan University and Collaborative Innovation Center of Biotherapy, Chengdu 610041, China

[4] Key Laboratory of Birth Defects and Related Diseases of Women and Children, Division of Neurology, Department of Paediatrics, West China Second University Hospital, Sichuan University, Chengdu 610041, China

of serine synthesis is the conversion of 3-phosphoglycerate (3-PG) to 3-phosphohydroxypyruvate (3-PHP), a process that is catalyzed by 3-phosphoglycerate dehydrogenase (PHGDH), an NAD^+-dependent enzyme [5].

PHGDH is overexpressed in 16% of all cancers and diverse cancer types, including breast, melanoma, lung, colon, and pancreatic cancers [4]. PHGDH overexpression often leads to higher cell proliferation and greater metastasis, correlates with poor prognosis, and may cause drug resistance [6, 7]. The downregulation of PHGDH is reported to inhibit high PHGDH-expressing cell lines, but has less effect on low PHGDH-expressing cell lines [5, 8, 9]. Therefore, PHGDH is increasingly considered as a promising anticancer drug target.

Several PHGDH inhibitors have been recently reported, including CBR-5884, NCT-503, PKUMDL-WQ-2101, ixocarpalactone A, α-ketothioamide derivatives, disulfiram, azacoccone E, indole amides and BI-4924 [9–18]. However, none of these inhibitors have entered clinical trials [4, 19]. One possible cause of the problem is the lack of enzyme property knowledge, e.g., how the enzyme activity is allosterically regulated and what are the critical residues that influence its activity. Except for BI-4924 that binds to the NAD^+ binding pocket [13], due to the lack of complex structures, it is largely unclear how the remaining inhibitors bind to PHGDH.

In this work, the natural product oridonin was identified as a new PHGDH inhibitor. Oridonin is an ent-kaurane diterpenoid isolated from *Rabdosia rubescens*, and it exhibits diverse biological activities including anti-cancer and anti-inflammation effects [20, 21]. The investigation on oridonin inhibition mechanism led to the discovery of new biophysical and biochemical properties of PHGDH. The crystal structure indicated that oridonin covalently bound to C18, resulting in a decrease in substrate affinity. Biochemical analysis showed that PHGDH activity was intolerant to SBD cysteine mutations. Inhibitor binding could not only inhibit PHGDH enzyme activity but also reduce its stability, promote its aggregation in vitro and its degradation in cells. Unexpectedly, most of the tested PHGDH cancer mutants were less active than the wild-type protein.

Materials and methods

Chemicals

Oridonin was purchased from MCE (cat. NSC-250682, USA). Using high performance liquid chromatography (HPLC–MS), oridonin was determined to be > 99% pure by the manufacturers and > 97% pure by our ^{1}H NMR [22]. The tris(2-carboxyethyl)phosphine (TCEP, C4706), iodoacetamide (IAM, V900335) were all purchased from Sigma-Aldrich (USA). The optima LC–MS acetonitrile (A955-4), methanol (A456-4), formic acid (A117-50) and water (W6-4) were purchased from Thermo Fisher Scientific (USA).

Cloning, protein expression and purification

The full length human PHGDH, sPHGDH (3–314 a. a.), and mutants were cloned into a pET-28a expression vector with an N-terminal His-tag fusion. Expression of these proteins was induced by addition of 0.1 mM isopropyl β-D-1-thiogalactopyranoside (IPTG) in *E. coli* BL21 (DE3) cells and cultured for 15 h at 18 °C in LB Broth (Miller). Cells were harvested and sonicated in a buffer containing 50 mM Tris–HCl pH 8.0, 10 mM Imidazole pH 8.0, 300 mM NaCl, 5 mM $MgCl_2$, and 1 mM PMSF. After centrifugation, the supernatants were purified on a Ni–NTA column and eluted in a buffer containing 300 mM imidazole pH 8.0, 150 mM NaCl, 5 mM $MgCl_2$, and 1 mM beta-mercaptoethanol (BME). The eluted proteins were further purified by Q-sepharose anion exchange chromatography (low salt buffer: 30 mM Tris pH 8.0, 1 mM DTT; high salt buffer: 1 M NaCl) and a Superdex 200 Increase gel filtration column in buffer containing 25 mM HEPES pH 7.5 and 200 mM NaCl. The folding of mutants was checked by differential scanning fluorescence assay.

In vitro PHGDH enzyme activity measurement and inhibitor screening assay

PHGDH activity was measured in 96-well plates (100 µL per well) at room temperature by monitoring Resorufin fluorescence (Ex 544 nm/Em 590 nm) with a BioteK plate reader. Hydrazine sulfate was added to prevent product inhibition. Assays were performed in a reaction buffer containing 30 mM Tris pH 8.0, 1 mM EDTA, 0.1 mM 3-PG, 20 µM NAD^+, 1 mM hydrazine sulfate, 0.1 mM resazurin, and 0.0001 enzyme unit of diaphorase per 100 µL reaction, unless specified. Hydrazine sulfate was used to eliminate the product 3-PHP (Fig. S1). To test PHGDH enzyme activity, each mutant (100, 200 and 400 nM) was directly mixed with the reaction buffer for 2 h before measurement. For the primary screening assay, 200 nM sPHGDH was pre-incubated with 5 µM of different small molecules for 2 h. Fluorescence was measured after another 2 h of reaction. For the IC_{50} measurements, 200 nM sPHGDH was pre-incubated with different concentrations of oridonin. Triton X-100 did not influence the IC_{50} of oridonin (Fig. S2).

Isothermal titration calorimetry (ITC)

The ITC experiment was performed in a buffer containing 25 mM Tris pH 8.0 and 1 mM EDTA using a MicroCal

iTC200 instrument (GE Healthcare). sPHGDH at 200 μM concentration was titrated into 150 μM oridonin by 19 × 2 μL injections with 120 s spacing between injections. The thermodynamic parameters of binding were determined using ORIGIN version 7.0 (OriginLab), fitting a one-site model.

Cell viability assay

MDA-MB-468 and A2780 cells were maintained in Dulbecco's modified Eagle's medium (Hyclone) supplemented with 10% (v/v) fetal bovine serum (Biological Industries). MGC803 cells were cultured in Roswell Park Memorial Institute (RPMI) 1640 medium supplemented with 10% (v/v) fetal bovine serum. Cell viability assays were performed in 96-well plates, seeding 1000 cells each well. Different concentrations of oridonin (0.4–12.5 μM) or other inhibitors (1.56–50 μM) were added 15 h later. After another 72 h, cells were stained with sulforhodamine B (SRB).

EdU cell proliferation assay

EdU cell proliferation assay was performed using a Beyo-Click™ EdU Cell Proliferation Kit with Alexa Fluor 488 (Beyotime). MDA-MB-468 cells were seeded in 24-well plates and cultured for 24 h. After 8 h of oridonin treatment, cells were incubated with EdU for 2 h before being fixed. Images were acquired by an Olympus CKX53 confocal microscope, and analyzed using NIH ImageJ and Graphpad software. For one sample, six regions each containing at least 30 cells were analyzed for the percentage of EdU positive cells. The statistical significance was calculated by one-way ANOVA test in GraphPad.

Western blot

MDA-MB-468 cells were cultured using 6-well plates. Cells were harvested with 1X SDS-PAGE loading buffer and analyzed by western blot using antibodies against PHGDH (ProteinTech, 1:1000), PARP (ProteinTech, 1:1000), and β-actin (ProteinTech, 1:1000). Goat Anti-Mouse IgG (Signalway Antibody, 1:5000) was used as the secondary antibody.

Cellular thermal shift assay (CETSA)

MDA-MB-468 cells were cultured to 50% confluence in 10 cm culture dishes and collected in PBS. Cells were lysed and centrifuged to remove cell debris. Supernatants were incubated with 40 μM oridonin or DMSO and then heated at different temperatures for 3 min. The heated samples were centrifuged, and the supernatants were analyzed by western blot.

X-ray crystallography

Crystals of sPHGDH (10 mg/mL) were screen by hanging drop vapor diffusion. A slightly better shaped sPHGDH crystal formed in 0.2 M Na formate, and 20% w/v PEG 3350 at 20 °C. The sPHGDH crystals were soaked in crystallization buffer containing 1 mM oridonin for 2 h. Crystals were cryo-protected in soaking buffer supplemented with 20% (wt/vol) PEG400 before freezing in liquid nitrogen. X-ray diffraction data were collected at Shanghai Synchrotron Radiation Facility (SSRF) beamlines BL17U1 and BL19U1. Coordinates of PHGDH (pdb code: 2G76) were used as the search model to solve the inhibitor complex. The data collection and refinement statistics are provided in Table 1.

Table 1 Crystal data collection and refinement statistics

	sPHGDH:oridonin
Cell axial lengths (Å)	$a=43.18$, $b=126.47$, $c=59.29$ $\alpha=\beta=\gamma=90$
Space group	$P2_1$
Data collection	
Resolution range (Å)	50.00–1.70 (1.73–1.70)
Number of observed reflections	352,344 (11,348)
Number of unique reflections	66,526 (2702)
Completeness (%)	96.7 (78.3)
Redundancy	5.3 (4.2)
R_{pim}	0.034 (0.439)
Highest shell CC1/2	0.665
Mean I/I_{sigma}	18.5 (1.7)
Refinement	
Resolution range (Å)	43.0–1.70 (1.74–1.70)
Number of working reflections	63,125 (3806)
Number of test reflections	3284 (182)
R_{work} [a]	0.135 (0.250)
R_{free} [b]	0.171 (0.252)
R.m.s. deviation bond lengths (Å)	0.004
R.m.s. deviation bond angles (°)	1.303
Average B-factors (Å2) (# of atoms)	48.1 (5264)
Ramachandran plot	
Most favored regions (%)	91.5
Allowed regions (%)	8.1
General allowed regions (%)	0.4
Disallowed regions (%)	0.0

[a] $R_{work}=\Sigma|Fo - Fc|/|Fo|$, where Fc and Fo are the calculated and observed structure factor amplitudes, respectively

[b] R_{free} calculated as for R_{work}, but for 5.0% of the total reflections chosen at random and omitted from refinement for all data sets

Mass spectrometry analysis

For mass spectrometric analysis, sPHGDH (1 μM) was incubated with different concentrations of oridonin (1 μM, 5 μM, 25 μM) for 1 h at room temperature. After removing free oridonin from samples using ultracentrifugation, the proteins were precipitated with four volumes of precooled acetone. The precipitate was collected, washed, and digested by trypsin overnight. TCEP and IAM were used for reductive alkylation of peptides. After being desalted, all peptide samples were lyophilized and resuspended in buffer A (2% acetonitrile and 0.1% formatic acid), and LC–MS/MS analysis was performed using an EASY-nLC 1000 nanoflow LC instrument coupled to a Q-Exactive quadrupole-orbitrap mass spectrometer (Thermo Fisher Scientific). The raw files acquired using the Q-Exactive plus were analyzed and searched against the sPHGDH sequence using Sequest HT search engine on Proteome Discovery (PD 2.3, Thermo). Oxidation of methionine, cysteine carbamidomethylation and cysteine oridonination (C_{ori}) were set as variable modifications. The peptide false discovery rate (FDR) was calculated with searches against the corresponding reverse database. Peptides with an expectation value < 1% FDR were chosen for further data processing.

Differential scanning fluorescence assay

For the differential scanning fluorescence assay, sPHGDH (20 μM) was incubated with 100 μM oridonin or DMSO buffer for 0.5 h in 0.2 mL strip tubes. The assay buffer contains 30 mM Tris pH 8.0 and 1 mM EDTA. Next, 5 × SYPRO® Orange (Thermo) was added to the samples. The samples were heated in a CFX96 Real-time System (BioRad) from 25 to 95 °C in 0.5 °C steps. The data were processed with CFX Manager software and GraphPad. The stain was excited at 470 nm and the emission at 570 nm was measured. Experiments were performed three times with duplicate wells for each experiment.

GTA cross-linking assay

For GTA cross-linking, sPHGDH (5 μM) was incubated with oridonin (0, 1.25, 2.5, 5, 10, or 20 μM) in buffer containing 20 mM PBS and 100 mM NaCl. After overnight incubation at 4 °C, the protein was cross-linked for 2 h in the presence of GTA (0.05% v/v) at 37 °C. The reaction was then quenched by addition of 0.5 M Tris pH 8.0. Samples were separated by SDS-PAGE and stained with Coomassie stain for 1 h.

Results

Identification of oridonin as a natural product inhibitor of PHGDH

A high-throughput screening assay was adapted from a former report [9], in which the product NADH was measured indirectly through a coupling reaction (Fig. 1A). A short fragment (sPHGDH) containing the substrate-binding domain (SBD) and the NAD-binding domain (NBD) was used in the screen since it is more stable than the full length protein [23]. Nine initial hits (more than 90% inhibition) were identified from a screen of about 300 proprietary natural products (Fig. 1B). Counter-screening against the coupling enzyme diaphorase yielded two PHGDH-specific inhibitors, oridonin and withaferin A (Fig. 1B). Withaferin A is structurally similar to the reported PHGDH inhibitor ixocarpalactone A [12], we thus mostly focused on oridonin in the following studies (Fig. 1C). In an enzyme assay, the half-inhibitory concentration (IC_{50}) of oridonin (0.48 ± 0.02 μM) was similar to that of CBR-5884 (0.73 ± 0.02 μM) [9], but lower than that of NCT-503 (3.63 ± 0.10 μM) (Fig. S3) [10]. In PHGDH-high MDA-MB-468 cells, oridonin (2.49 ± 0.56 μM) was about tenfold more potent than CBR-5884 (21.99 ± 0.58 μM), NCT-503 (20.63 ± 1.02 μM), and BI-4916 (18.24 ± 1.06 μM) (Fig. S4) [13].

The direct binding between oridonin and sPHGDH was verified by isothermal titration calorimetry (ITC) (Fig. 1D). The calculated *N* value (0.16 ± 0.03 μM) suggested binding of each sPHGDH to six to seven molecules of oridonin (see later sections). Pre-incubation of sPHGDH with oridonin for different lengths of time prior to reaction showed that oridonin inhibited the enzyme activity in a time-dependent manner (Fig. 1E). Thus, oridonin likely bound to PHGDH covalently through its reactive alpha–beta unsaturated ketone group. Progress curve analysis suggested that oridonin was a slower binder compared with CBR-5884 (Fig. S5) [24].

Crystal structure of PHGDH in complex with oridonin

To elucidate the mechanism of PHGDH inhibition, different inhibitors (including oridonin, NCT-503, and CBR5884) were soaked with sPHGDH crystals, but only the complex crystal structure of oridonin-sPHGDH was obtained. The structure was solved using the previously deposited malate-bound sPHGDH (PDB code: 2G76), with a homodimer in each asymmetric unit (Fig. S6A and Table 1). In the structure, oridonin's α, β-unsaturated ketone binds covalently to the sulfhydryl of C18 (Fig. 2A), which is the most exposed cysteine in sPHGDH (Table 2). Additionally, oridonin formed hydrogen bonds with the E297 side chain and made

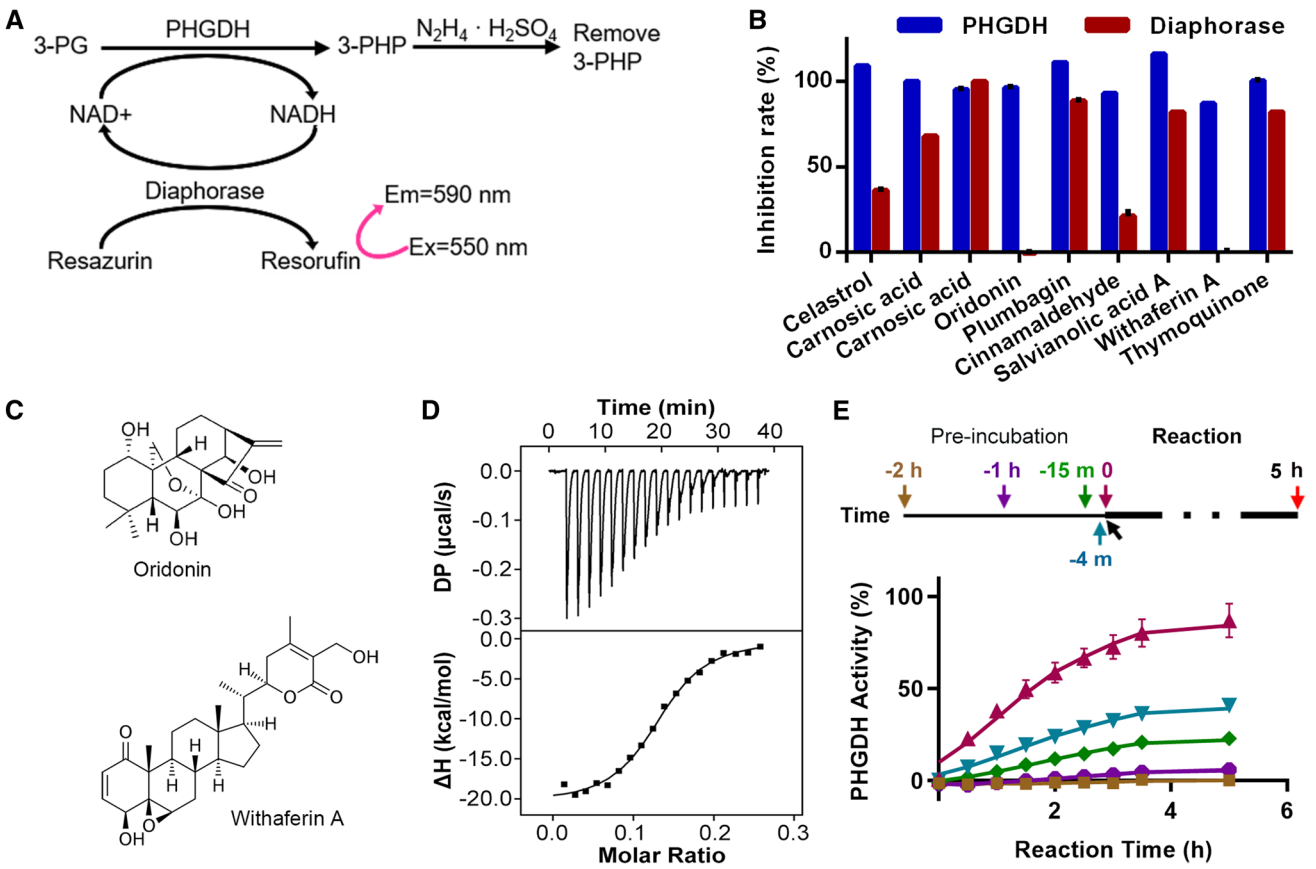

Fig. 1 Identification of oridonin as a natural product PHGDH inhibitor. **A** The in vitro inhibitor screening assay. Diaphorase couples the generation of NADH to the generation of fluorescent resorufin. Hydrazine sulfate ($N_2H_4 \cdot H_2SO_4$) prevents product feedback inhibition of PHGDH by removing 3-phosphohydroxypyruvate (3-PHP). **B** Inhibition rate against PHGDH and diaphorase by the hit compounds (5 μM, > 90% PHGDH inhibition), from one triplicate experiment. The hits were pre-incubated with diaphorase or PHGDH for 2 h before enzyme activity measurement. **C** The chemical structure of oridonin and withaferin A. **D** Isothermal titration analysis. PHGDH (200 μM) was titrated into 150 μM oridonin at 20 °C. **E** Time-dependent PHGDH inhibition. Samples of 200 nM PHGDH were pre-incubated with 1 μM oridonin for the indicated times, and then PHGDH activity was monitored for 5 h. The time line is shown above. Black arrow indicates the start of the reaction. The data are normalized to the 5 h reading of the '0 min' pre-incubated enzyme. A short fragment of PHGDH (sPHGDH, a.a. 3–314) containing only the NAD-binding domain (NBD) and the substrate-binding domain (SBD) was used in these experiments. Data are expressed as mean ± standard error of mean (SEM), $n = 3$

hydrophobic contacts with K21, I22, and D25 side chains (Fig. 2A). The electron density only allowed modeling of oridonin in one chain of the PHGDH dimer (Fig. S6B). The other chain displayed a weak and discontinuous electron density beyond C18 (Fig. S7), suggesting that this 'oridonin' may have a lower occupancy or have a very high flexibility, or may not be covalently bond.

PHGDH substrate affinity may be regulated through C18 and R54

Due to steric clash, oridonin binding induced a reposition of C18 sulfhydryl (4.5 Å shift) and the associated α1 helix (Fig. 2B). Concomitantly, the substrate-binding domain twisted away from NADH (Movie 1), rendering the substrate-binding pocket more exposed (Fig. S8). Further, the guanidine group of R54, which directly binds to the substrate analog malate in 2G76, shifted 5.6 Å toward the α1 helix, and formed hydrogen bonds with the main chain carbonyls of S14, A76, and Q292 (Fig. 2B). Surface representation shows that R54 is optimally docked/locked into a newly formed channel in the oridonin-bound SBD structure (Fig. 2C). This R54 docking/sequestration is not due to the lack of substrate analog, because R54 guanidine docking is not observed in any other substrate-free PHGDH structures (Fig. S9) [14]. The sequence conservation of R54 (Fig. S10) suggests that it may play a role in catalysis.

To test whether R54 sequestration hampers the enzyme activity, we constructed three mutants of sPHGDH, namely, C18W and C18Y to simulate the binding effect of oridonin on C18 [25] and R54A that is potentially impaired in substrate interaction. While C18W and C18Y were thermally

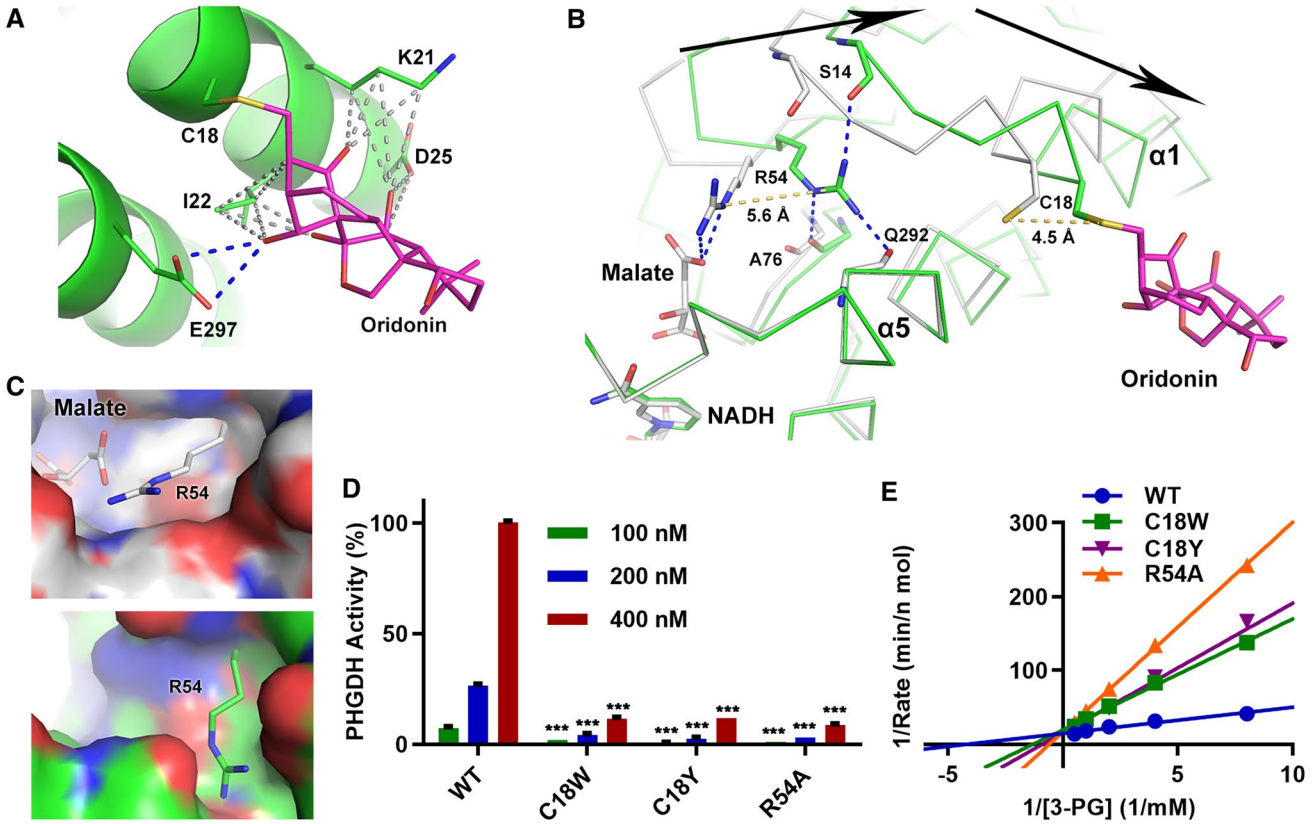

Fig. 2 Co-crystal structure of sPHGDH:oridonin reveals a mechanism of PHGDH inhibition by R54 reposition. **A** Zoomed view of sPHGDH and oridonin interaction. Interacting residues are shown as green sticks. Hydrogen bonds and hydrophobic contacts are denoted as blue and gray dashed lines, respectively. **B** Relocation of C18 sulfhydryl and R54 guanidine group (yellow dashed lines) upon oridonin binding. Oridonin-bound sPHGDH (green) is superimposed onto the malate-bound sPHGDH (2G76, gray) using the NBD atoms. Hydrogen bonds are shown as blue dotted lines. For clarity, the side chains of S14, A76, and Q292 are not displayed. **C** Surface and stick representation of the active site around R54 in 2G76 (up) and the oridonin complex (down). **D** Enzyme activity comparison of WT, C18W, C18Y, and R54A at 100, 200, and 400 nM concentrations. Data are normalized to the reading of the 400 nM WT sample. Statistical differences relative to the WT sample at the same concentration are compared. $*p<0.05$ and $***p<0.001$. **E** Lineweaver–Burk double reciprocal plots for WT, C18W, C18Y, and R54A

less stable and R54A was more thermally stable compared with WT (Fig. S11). At 400 nM sPHGDH concentration, C18W and R54A lost 91% and 82% enzyme activity compared with wild type (WT) (Fig. 2D). Compared with WT, the maximal reaction rates (Vmax) changed only slightly, but the Michaelis constant K_M values for 3-PG were notably increased by C18W (3.9 folds), C18Y (4.0-fold), and R54A (8.1-fold) (Fig. 2E and Table S1). The relatively smaller change in K_M measured for C18W and C18Y argues that the nature of R54 sequestration may be dynamic/partial in solution. Besides, C18W exhibited much reduced stability of enzyme activity compared with WT (Fig. S12), which may explain the observed small reduction of Vmax (Table S1).

Multiple cysteines in PHGDH could be targeted

If C18 is the only binding site of oridonin in sPHGDH, a mutant C18S is expected to abolish the inhibition of oridonin. Results showed that C18S was completely inhibited by oridonin (Fig. 3A), suggesting that there were more binding sites in PHGDH. It should be noted that C18S showed dramatically reduced enzyme activity and stability (Fig. 3B and S12), indicating that PHGDH activity was very sensitive to small changes at this site. To search for other PHGDH-binding sites, sPHGDH was incubated with different concentrations of oridonin (1 μM, 5 μM, and 25 μM) for 1 h before being analyzed by MS. At a low oridonin concentration (1 μM), only C18 (or C19, but not simultaneous) and C281 were observed to be conjugated (Fig. 3C). The number of binding sites gradually increased as the oridonin concentration increased, and at the highest oridonin concentration (25 μM), the identified sites included C18 (or C19), C48, C254 and C281 (Fig. 3C, Fig. S13). Although even higher concentrations of oridonin treatment might lead to more modified sites, in view of

Table 2 Summary table of studies on the sPHGDH cysteines

Mutation	Location	SAA[a] (Å^2)	Bound in[e]	C to S mutant		C to W mutant	
				Activity (%)[b]	IC_{50} (μM)[c]	Activity (%)[b]	Soluble (%)[d]
C18	SBD	31.1	Crystal and MS	11	0.31 ± 0.01	9	64
C19	SBD	0.7	MS	5		1	77
C48	SBD	0.2	MS	2		0	60
C111	NBD	2.7	None				
C116	NBD	0.0	None				
C200	NBD	0.0	None	120	0.43 ± 0.01	0	6
C225	NBD	0.0	None	92	0.51 ± 0.03	13	19
C234	NBD	12.3	None				
C254	NBD	0.0	MS	87	0.46 ± 0.02	0	10
C281	NBD	0.0	MS	129	0.44 ± 0.01	0	58
C295	SBD	0.0	None	23		4	75

[a]Solvent accessible area

[b]As determined with 400 nM sPHGDH, treating WT activity as 100%

[c]The IC_{50} values were measured with 200 nM sPHGDH, except for C18S at 400 nM concentration. IC_{50} of WT is 0.48 ± 0.02 μM

[d]The soluble fraction for the *E. coli* expressed sPHGDH. The soluble fraction of WT is 92%

[e]MS cannot differentiate whether C18 or C19 was conjugated, but their simultaneous conjugation was not detected. Shown is the binding sites for 25 μM of oridonin

the crystal structure data, C18 and C281 were considered the most easily conjugatable positions.

PHGDH activity can also be inhibited through the additional cysteines

Even though both ITC and mass spec showed that multiple cysteines can be bound by oridonin, it is unclear whether oridonin's binding to each cysteine could elicit an inhibitory response. Therefore, all cysteines (except for C111, C116, and C234) were individually mutated to tryptophans (W) to mimic the binding of oridonin to each site. C200W and C254W were totally insoluble, but the other C to W mutants were sufficiently soluble to purify (Fig. S14). While C19W and C48W showed reduced thermal stability, C281W showed increased thermal stability (Fig. S11). Similar to C18W, the purified mutants all exhibited very low activities (Fig. 3D). This suggests that the binding of oridonin and other covalent inhibitors to these cysteine residues would inhibit PHGDH.

SBD cysteines are more sensitive to isosteric mutations

To verify the MS-generated oridonin binding priority of different cysteines, we attempted to test the oridonin sensitivity of each C to S single mutant. Unfortunately, all the SBD single cysteine mutants C19S, C48S, and C295S were tremendously impaired in enzyme activity and thermal stability (Fig. 3E and S11), thus oridonin sensitivity could not be drawn for these sites. Although the NBD mutants were less thermally stable, they were active, and showed similar oridonin IC_{50} values compared with WT (Fig. 3F, S11, and Table 2). Attempts were also made to create multiple cysteine mutants or SBD cysteine mutants with other isosteric mutations (e.g., C to A or T or V). However, these mutants were either insoluble or inactive, impeding further analysis. These results suggest that the SBD cysteines were very sensitive to small perturbations.

3PG is more protective than NAD^+ toward oridonin inhibition

Efforts were also taken to test whether different PHGDH substrates may influence the IC_{50} of oridonin (no oridonin pre-incubation here). Results showed that increasing 3-PG concentration 100-folds increased oridonin IC_{50} by about sevenfold (3.4 μM vs. 23.0 μM) (Fig. 3G). The explanations for 3-PG protection may be that 3-PG inhibited the binding of oridonin to C18 through allostery, or binding to other buried cysteines, e.g., 3-PG may have promoted dimerization of PHGDH [24], which reduced the accessibility of dimer interface residue C281. In contrast, increasing NAD^+ concentration 200-folds only slightly increased the IC_{50} of oridonin (4.3 μM vs. 7.7 μM). As C234 is located in the NAD^+ pocket, it can be concluded that C234 is not a major oridonin binding site, in agreement with the MS data.

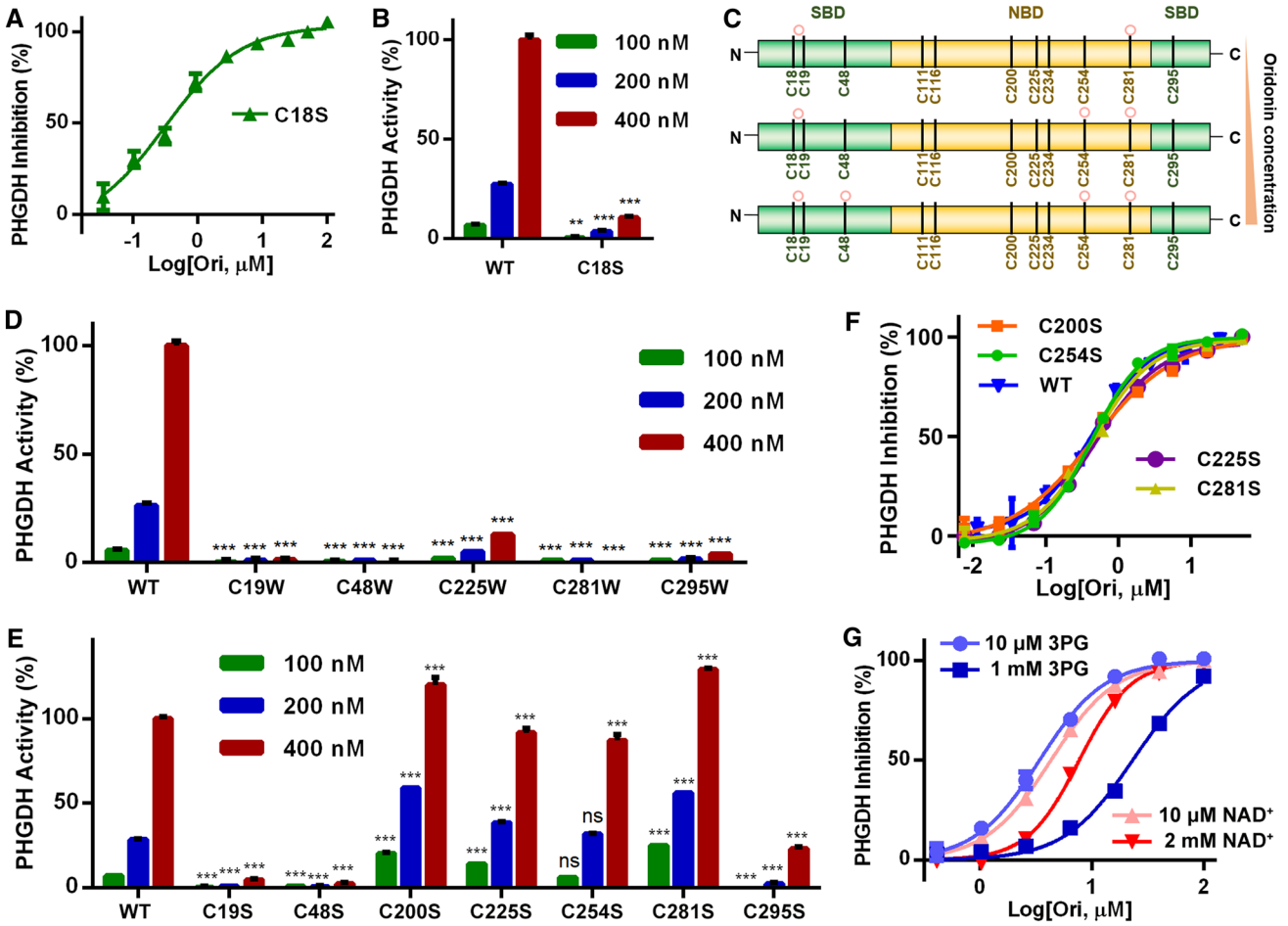

Fig. 3 PHGDH is very sensitive to cysteine mutations, especially those in the SBD. **A** Concentration-dependent enzyme inhibition analysis for C18S. C18S was used at 400 nM concentration. **B** Enzyme activity of WT and C18S in the absence of oridonin. **C** Location of oridonin-modified cysteines by mass spectrum analysis, at different concentrations of oridonin (1 μM, 5 μM and 25 μM). MS2 spectrum could not differentiate whether C18 or C19 was conjugated, but their simultaneous conjugation was not detected. **D** Enzyme activity of cysteine to tryptophan mutants. Statistical differences to the WT sample at the same concentration are compared. $^{**}p<0.01$; and $^{***}p<0.001$. **E** Enzyme activity of the cysteine to serine mutants. **F** Concentration-dependent enzyme inhibition analysis for WT, C200S, C225S, C254S, and C281S in sPHGDH. Data are expressed as mean ± SEM, $n=3$. **G** Oridonin IC_{50} analysis under different concentrations of 3-PG or NAD^+. In this enzyme assay, oridonin was not pre-incubation with sPHGDH

PHGDH is aggregated by different inhibitors

The fact that different mutations impaired PHGDH stability and solubility suggests that PHGDH is metastable and may be aggregated by inhibitors. Indeed, differential scanning fluorescence (DSF) showed that purified sPHGDH displayed reduced thermal stability in the presence of oridonin (Fig. 4A). Besides, PHGDH oligomerization was observed in the presence of oridonin and the cross-linking reagent glutaraldehyde (Fig. 4B). Size exclusion chromatography showed sPHGDH aggregation in the presence of oridonin and CBR-5884, but not NCT-503 (Fig. 4C). At a higher sPHGDH concentration (5 mg/mL), increasing the molar ratio of oridonin gradually induced its precipitation, and an oridonin to sPHGDH molar ratio of eight completely precipitated sPHGDH (Fig. 4D).

PHGDH may be inhibited via proteasome-mediated degradation in cells

The above studies have showed that PHGDH was targeted by oridonin in vitro, but how PHGDH is affected by oridonin in cells is unknown. A cellular thermal shift assay (CETSA) showed reduced thermal stability of endogenous PHGDH in the presence of oridonin (Fig. 5A), suggesting that PHGDH was directly targeted by oridonin in cells. Moreover, the endogenous PHGDH protein level progressively declined when cells were treated with increasing

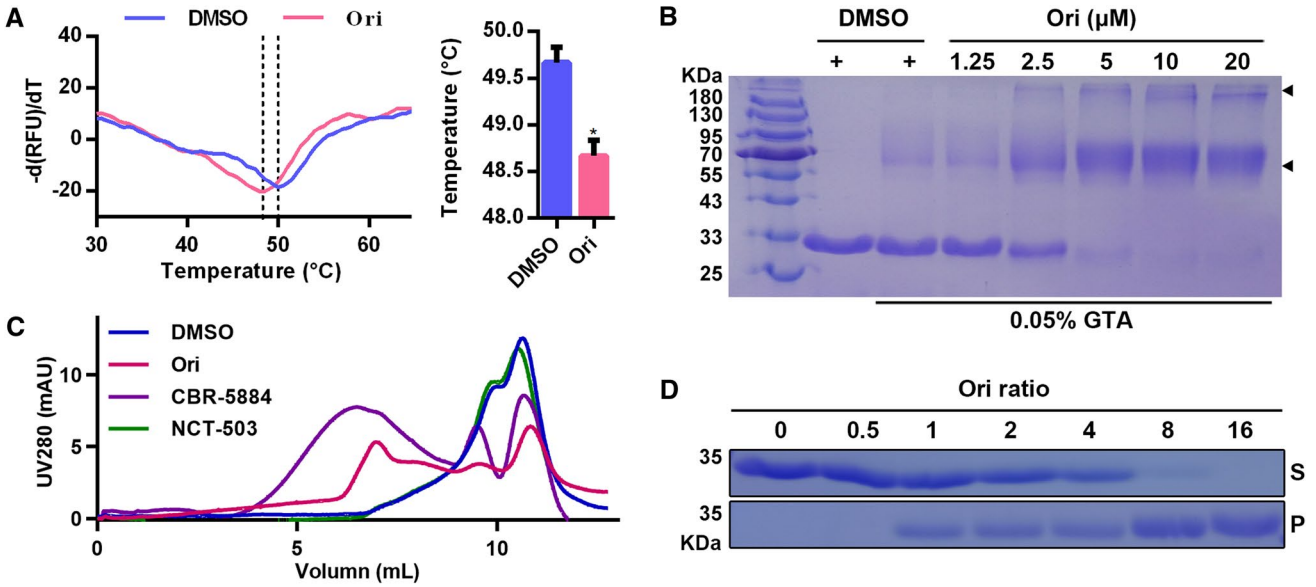

Fig. 4 PHGDH aggregates and precipitates in the presence of inhibitors. **A** First derivative of the melt curves of sPHGDH with DMSO or oridonin. The right panel shows the mean and standard error of measurements for three independent measurements. *$p < 0.05$. **B** Glutaraldehyde (GTA) cross-linking of sPHGDH. sPHGDH was pre-incubated with increasing concentrations of oridonin or DMSO overnight, and then cross-linked with GTA (0.05% v/v) for 2 h. Black arrows indicate cross-linked proteins. **C** Size exclusion chromatography profile for sPHGDH (20 μM) treated with DMSO- or different inhibitors (200 μM). Samples of sPHGDH were pre-incubated with DMSO or oridonin for 2 h on ice before size exclusion chromatography. **D** Precipitation of sPHGDH (5 mg/mL) upon binding to multiple oridonin molecules. Samples of sPHGDH were incubated with different molar ratios of oridonin (1:0.5, 1:1, 1:2, 1:4, 1:8, 1:16) at room temperature for 2 h. After centrifugation, the supernatant (S) and the pellet (P) fractions were analyzed by SDS-PAGE

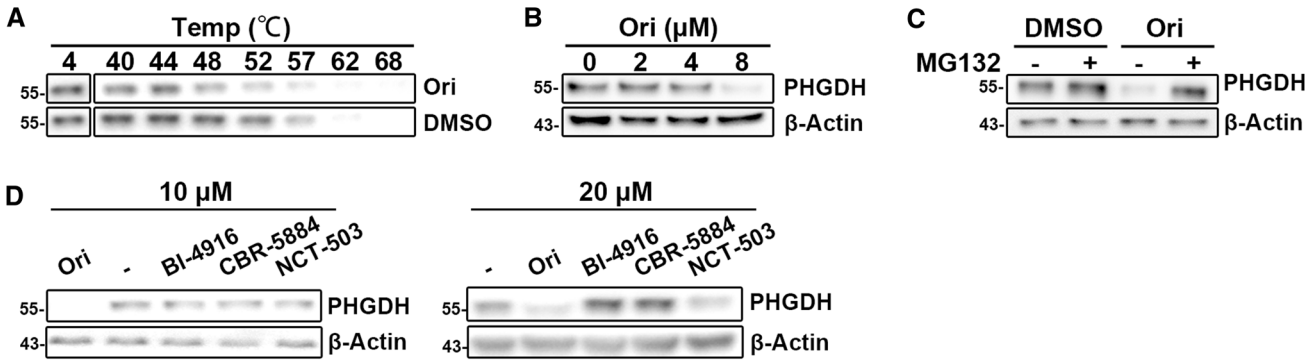

Fig. 5 PHGDH could be inhibited through degradation in MDA-MB-468 cells. **A** Thermal stability of endogenous oridonin in the presence of DMSO or oridonin (40 μM). The heated samples were centrifuged and the supernatants were analyzed by western bot. **B** Western blot analysis of intracellular PHGDH level. Cells were incubated with DMSO or various concentrations of oridonin for 48 h. **C** Endogenous PHGDH level in the presence of oridonin and the proteasome inhibitor MG132. Cells were treated with 10 μM oridonin or DMSO in the presence or absence of MG132 for 8 h. **D** Intracellular PHGDH level after treatment with different inhibitors for 48 h

concentrations of oridonin (Fig. 5B). The oridonin-mediated clearance of PHGDH was reversed by the addition of the proteasome inhibitor MG132, suggesting that the observed PHGDH clearance is proteasome-dependent (Fig. 5C). PHGDH degradation is specific for oridonin but not for CBR5884 and BI-4916 (Fig. 5D). NCT-503 was also able to induce PHGDH degradation at 20 μM concentration. Since PHGDH plays a role in serine (and downstream DNA) synthesis, we explored the cellular impact of PHGDH inhibition by oridonin. In agreement, increasing concentrations of oridonin gradually decreased the rate of DNA synthesis and the number of colonies formed in MDA-MB-468 cells (Fig. S15 and S16).

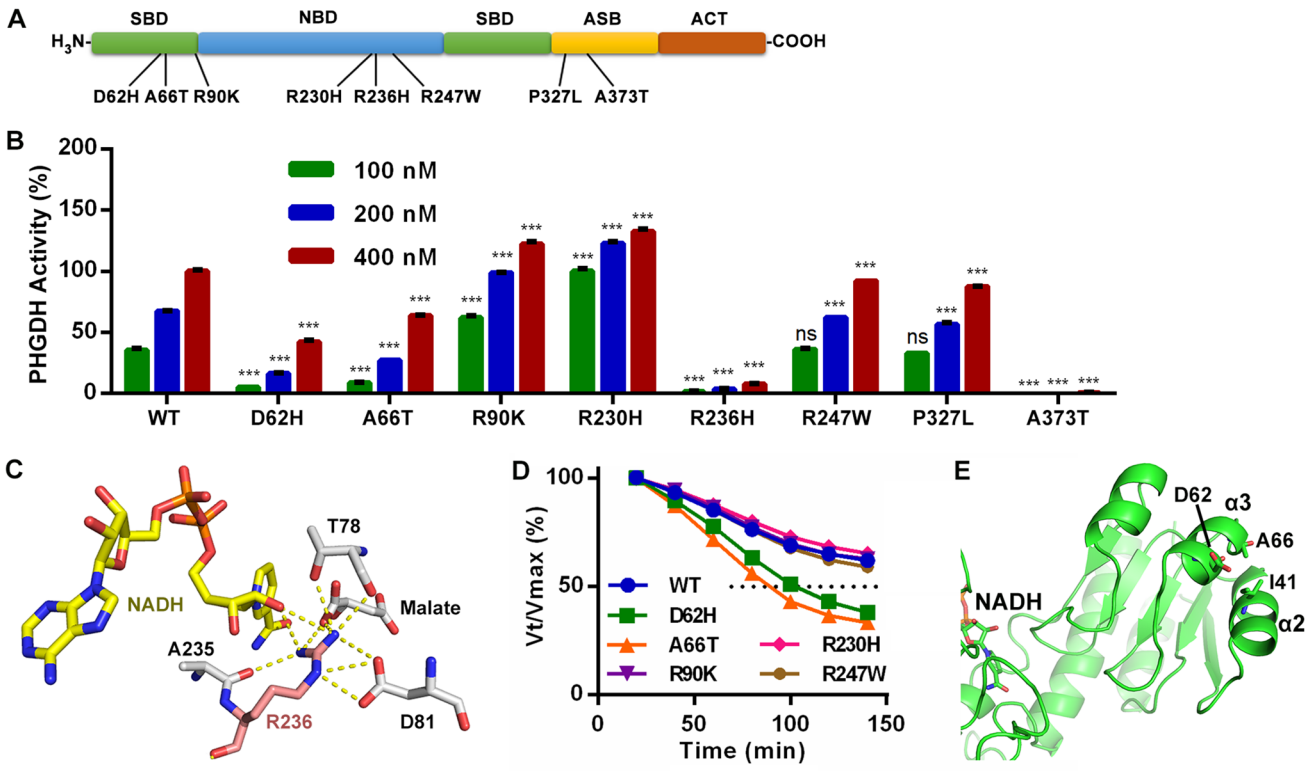

Fig. 6 PHGDH cancer mutants display altered enzyme activities. **A** Distribution diagram of selected PHGDH cancer mutations. **B** Enzyme activity of cancer mutants in full length PHGDH. Statistical differences relative to the WT sample at the same concentration are compared. ***$p < 0.001$. **C** Interaction between R236 (pink) and NADH (yellow), substrate analogue malate, SBD residues T78 and D81, and NBD residue A235. Dotted lines denote hydrogen bonds. **D** Vmax-normalized velocity (Vt) vs. time for cancer mutants (200 nM). Data are expressed as mean ± SEM, $n = 3$. **E** Location of D62 and A66 and their surrounding environment. PHGDH is shown as a cartoon and critical residues are shown as sticks

PHGDH cancer mutants display altered enzyme activities

Mutation is often employed by cancer cells to gain proliferative benefit, but how PHGDH cancer mutations affect its activity is unknown. From the COSMIC database, eight missense cancer mutations (count ≥ 2) including D62H, A66T, R90K, R230H, R236H, R247W, P327L, and A373T were selected and cloned into the full length PHGDH, expressed, and purified (Fig. 6A). Mutants R90K and R230H showed increased enzyme activities, while the other six displayed decreased activities (Fig. 6B), and the enzyme activities of R236H and A373T were barely detectable. In the crystal structure, R236 forms key contact with malate, NADH, and the substrate-binding domain (Fig. 6C). Therefore, the R236 mutation would be expected to compromise its enzyme activity. The activity reduction of A373T is consistent with a previous report [26], but it is unclear how it exactly inhibits PHGDH without the full length protein structure. The lower stability of D62H and A66T (Fig. 6D) may account for the reduction of activity for these two mutants (Fig. 6B). D62 is at the positive end of a short helix (α3), and mutating to an H may reduce the stability of this helix (Fig. 6E). A66 is in close contact with I41 in α2, a T mutation may disrupt the interaction. The NBD and SBD mutations were also cloned into the more stable fragment sPHGDH. Except R236H, the other mutants were less thermally stable (Fig. S11). The mutational effects were similar in full length PHGDH or sPHGDH (Fig. S17, correlation coefficient of 0.89). All mutants remained sensitive to oridonin (Fig. S18, Table S2), consistent with the finding that oridonin could inhibit PHGDH through binding to different cysteines.

Discussion

In addition to displaying the Warburg effect, cancer cells also engage metabolic reprogramming to facilitate the accumulation of precursors for nucleotide, lipid, and amino acid synthesis. PHGDH is a bottleneck enzyme in serine synthesis pathway and has received widespread interest in recent years [27, 28]. Serine withdrawal and genetic/pharmacological inhibition of PHGDH have shown promising results for the suppression of tumor growth [5, 10, 29, 30]. Despite

the identification of several PHGDH inhibitors, none have progressed into clinical trials and most of them have insufficient cellular potency [4, 18, 19]. In this work, oridonin was screened as a new PHGDH inhibitor with slightly improved potency (Fig. 1). Although oridonin is more potent in cells, the anti-cancer mechanism is unlikely to be solely due to PHGDH inhibition, as oridonin has been reported to bind to a number of cellular targets [31–33]. The promiscuous binding nature of oridonin renders it challenging to develop oridonin as a PHGDH-targeted therapy. However, there has been renewed interest in multi-targeting drugs and oridonin may be an important advance as more potent analogs are developed [34–36].

Previously, it has been reported that binding of the product serine to the regulatory domain (ACT) induced domain conformational changes and reduced Vmax in *Escherichia coli* PHGDH [37], but it is not clear how human PHGDH is allosterically regulated currently. Structure and biochemical analyses indicated that the binding of oridonin to C18 may reduce the affinity of 3-PG by sequestering R54 which interacts 3-PG (Fig. 2). Here again, a domain conformational change was observed, but unlike serine inhibition, Vmax was not affected by C18W. Thus, this new mechanism of allosteric inhibition is likely not employed by the serine inhibition mechanism in humans. In *Rabdosia rubescens* where oridonin is isolated from, the gene PHGDH does not exist, effectively preventing oridonin from threatening growth of the plant. The human PHGDH C18 pocket is slightly shallow, but the structure and mechanism information provided here may help future structure-based drug development, as has been done for targeting Ras-G12C [38].

Further analysis suggested that more cysteines could be conjugated by oridonin, and their W mutants were either insoluble or barely active (Table 2). Therefore, PHGDH would be inhibited if any of these sites were bound by an inhibitor capable of forming a covalent bond, including CBR-5884, PKUMDL-WQ-2101, ixocarpalactone A, disulfiram, DNS-pE, oridonin, and withaferin A. However, these sites would not be bound with equal propensity or priority, and different inhibitors may selectively use one or more sites. For example, it is reported that disulfiram binds to C111, C116 and C281 [16], and DNS-pE binds to C234, C281, and C295 [39]. We showed that the number of oridonin-binding sites depended on oridonin concentration, and at the closest concentration around enzyme assay IC_{50}, oridonin only bound to C18 (or 19) and C281 based on the MS results. It surfaces that the bound sites may be partially occupied. Also, due to the length and the ionization efficiency of digested peptides, some of the unmodified cysteine residues may also be bound, and the generated site priority (Fig. 3C) should be interpreted with caution.

ITC and MS indicated multiple binding sites, but the crystal structure only showed a single binding site. Compared with the solution state, protein in crystals is generally more rigid and less dynamic [40]. Thus, steric hindrance in crystals likely prevented excess oridonin from accessing the other less exposed cysteines during crystal socking. For example, oridonin binding to C281 would disrupt dimer formation and almost certainly disrupt crystal packing. When oridonin and sPHGDH were pre-incubated before crystallization (rather than soaking), PHGDH either precipitated or formed no crystals, which disallowed the visualization of oridonin binding modes to other cysteines.

It should be noted that some of the mutations have inhibited enzyme activity through impairing protein folding rather than perturbing enzyme reaction directly, as indicated by the Tm reductions (S11). Since these cysteines (except C18) are mostly buried in the protein, its C to W mutations (or binding to inhibitors) will almost certainly disrupt local folding. In addition to impairing folding, due to its hydrophobicity, oridonin can increase the hydrophobicity of conjugated proteins, thereby promoting protein aggregation. Besides PHGDH, oridonin was reported to degrade a few proteins including BCL-ABL, Glut1, MCT1, and FAS [41–43]. The protein aggregation phenomenon may explain the reduction of endogenous protein levels observed in cells treated with oridonin (Fig. 5B), since cellular aggregates are usually targeted and eliminated by the degradation machineries [44].

Although PHGDH overexpression has been reported in cancers [5, 7], it is unknown whether PHGDH cancer mutations affect its activity. Testing the cancer mutations showed that PHGDH activity is very sensitive to small perturbations (Fig. 6B). Surprisingly, the activity of most cancer mutants is reduced compared to the WT protein. This seems to contradict the reports that cancer cells require more serine or higher serine synthesis activity [5, 29, 45]. Several studies have suggested non-metabolic roles of PHGDH in cancer [4, 46, 47]. Although the mutation frequency is quite low, cancer cells containing less active PHGDH mutants may take advantage of the non-metabolic functions of PHGDH instead of its enzyme activity. Thus, PHGDH inhibitors that only inhibit enzyme activity may not be suitable for the treatment of cancer subtypes with reduced PHGDH activity. Approaches that can induce PHGDH clearance, such as PROTAC, may still be useful for these cancer cells.

Supplementary Information The online version contains supplementary material available at https://doi.org/10.1007/s00018-021-04022-2.

Acknowledgements We thank the staffs from BL17B1/BL18U1/BL19U1/BL19U2/BL01B beamline of National Facility for Protein Science in Shanghai (NFPS) at Shanghai Synchrotron Radiation Facility, for assistance during data collection [48]. We appreciate Dr. Xiaofei Shen for providing resources and technical assistances.

Author contributions QS and YT conceived the project and prepared the manuscript. YT, XZ, YG, and KG performed all the experiments.

QS, YZ, LD, YL, and DJ supervised the project, and/or provided relevant resources.

Funding YZ is funded by the National S&T Major Project (2018ZX09201018), and LD is funded by the program of National Clinical Research Center for Geriatrics of West China Hospital (No. Z20191001).

Availability of data and material The resulting model has been deposited in Protein Data Bank with the accession code 7DKM. The MS raw data has been deposited into the ProteomeXchange Consortium (http://proteomecentral.proteomexchange.org) via the iProX partner repository with a dataset identifier of PXD029445 [49].

Declarations

Conflict of interest The authors declare that they have no conflicts of interest with the contents of this article.

Code availability Not applicable.

Ethics approval Not applicable.

Consent to participate Not applicable.

Consent for publication All authors have read and approved the manuscript for publication.

References

1. Hanahan D, Weinberg RA (2011) Hallmarks of cancer: the next generation. Cell 144:646–674
2. Mattaini KR, Sullivan MR, Vander Heiden MG (2016) The importance of serine metabolism in cancer. J Cell Biol 214:249–257
3. Hosios AM, Hecht VC, Danai LV, Johnson MO, Rathmell JC, Steinhauser ML, Manalis SR, Vander Heiden MG (2016) Amino acids rather than glucose account for the majority of cell mass in proliferating mammalian cells. Dev Cell 36:540–549
4. Zhao X, Fu J, Du J, Xu W (2020) The role of D-3-phosphoglycerate dehydrogenase in cancer. Int J Biol Sci 16:1495–1506
5. Possemato R, Marks KM, Shaul YD, Pacold ME, Kim D, Birsoy K, Sethumadhavan S, Woo HK, Jang HG, Jha AK et al (2011) Functional genomics reveal that the serine synthesis pathway is essential in breast cancer. Nature 476:346–350
6. Song Z, Feng C, Lu Y, Lin Y, Dong C (2018) PHGDH is an independent prognosis marker and contributes cell proliferation, migration and invasion in human pancreatic cancer. Gene 642:43–50
7. Zhu J, Ma J, Wang X, Ma T, Zhang S, Wang W, Zhou X, Shi J (2016) High expression of PHGDH predicts poor prognosis in non-small cell lung cancer. Transl Oncol 9:592–599
8. Jing Z, Heng W, Xia L, Ning W, Yafei Q, Yao Z, Shulan Z (2015) Downregulation of phosphoglycerate dehydrogenase inhibits proliferation and enhances cisplatin sensitivity in cervical adenocarcinoma cells by regulating Bcl-2 and caspase-3. Cancer Biol Ther 16:541–548
9. Mullarky E, Lucki NC, Beheshti Zavareh R, Anglin JL, Gomes AP, Nicolay BN, Wong JC, Christen S, Takahashi H, Singh PK et al (2016) Identification of a small molecule inhibitor of 3-phosphoglycerate dehydrogenase to target serine biosynthesis in cancers. Proc Natl Acad Sci USA 113:1778–1783
10. Pacold ME, Brimacombe KR, Chan SH, Rohde JM, Lewis CA, Swier LJ, Possemato R, Chen WW, Sullivan LB, Fiske BP et al (2016) A PHGDH inhibitor reveals coordination of serine synthesis and one-carbon unit fate. Nat Chem Biol 12:452–458
11. Wang Q, Liberti MV, Liu P, Deng X, Liu Y, Locasale JW, Lai L (2017) Rational design of selective allosteric inhibitors of PHGDH and serine synthesis with anti-tumor activity. Cell Chem Biol 24:55–65
12. Zheng M, Guo J, Xu J, Yang K, Tang R, Gu X, Li H, Chen L (2019) Ixocarpalactone A from dietary tomatillo inhibits pancreatic cancer growth by targeting PHGDH. Food Funct 10:3386–3395
13. Weinstabl H, Treu M, Rinnenthal J, Zahn SK, Ettmayer P, Bader G, Dahmann G, Kessler D, Rumpel K, Mischerikow N et al (2019) Intracellular trapping of the selective phosphoglycerate dehydrogenase (PHGDH) inhibitor BI-4924 disrupts serine biosynthesis. J Med Chem 62:7976–7997
14. Mullarky E, Xu J, Robin AD, Huggins DJ, Jennings A, Noguchi N, Olland A, Lakshminarasimhan D, Miller M, Tomita D et al (2019) Inhibition of 3-phosphoglycerate dehydrogenase (PHGDH) by indole amides abrogates de novo serine synthesis in cancer cells. Bioorg Med Chem Lett 29:2503–2510
15. Guo J, Gu X, Zheng M, Zhang Y, Chen L, Li H (2019) Azacoccone E inhibits cancer cell growth by targeting 3-phosphoglycerate dehydrogenase. Bioorg Chem 87:16–22
16. Spillier Q, Vertommen D, Ravez S, Marteau R, Themans Q, Corbet C, Feron O, Wouters J, Frederick R (2019) Anti-alcohol abuse drug disulfiram inhibits human PHGDH via disruption of its active tetrameric form through a specific cysteine oxidation. Sci Rep 9:4737
17. Ravez S, Corbet C, Spillier Q, Dutu A, Robin AD, Mullarky E, Cantley LC, Feron O, Frederick R (2017) alpha-ketothioamide derivatives: a promising tool to interrogate phosphoglycerate dehydrogenase (PHGDH). J Med Chem 60:1591–1597
18. Spillier Q, Ravez S, Unterlass J, Corbet C, Degavre C, Feron O, Frederick R (2020) Structure-activity relationships (SARs) of alpha-ketothioamides as inhibitors of phosphoglycerate dehydrogenase (PHGDH). Pharmaceuticals (Basel) 13:20
19. Ravez S, Spillier Q, Marteau R, Feron O, Frederick R (2017) Challenges and opportunities in the development of serine synthetic pathway inhibitors for cancer therapy. J Med Chem 60:1227–1237
20. Lu Y, Sun Y, Zhu J, Yu L, Jiang X, Zhang J, Dong X, Ma B, Zhang Q (2018) Oridonin exerts anticancer effect on osteosarcoma by activating PPAR-gamma and inhibiting Nrf2 pathway. Cell Death Dis 9:15
21. Huang W, Huang M, Ouyang H, Peng J, Liang J (2018) Oridonin inhibits vascular inflammation by blocking NF-kappaB and MAPK activation. Eur J Pharmacol 826:133–139
22. Lei Y, An Q, Zhang Y, Luo P, Luo Y, Shen X, Jia D, Sun Q (2020) Engineering chromosome region maintenance 1 fragments that bind to nuclear export signals. Protein Sci 29:1366–1372
23. Unterlass JE, Basle A, Blackburn TJ, Tucker J, Cano C, Noble MEM, Curtin NJ (2018) Validating and enabling phosphoglycerate dehydrogenase (PHGDH) as a target for fragment-based drug discovery in PHGDH-amplified breast cancer. Oncotarget 9:13139–13153
24. Xu H, Qing X, Wang Q, Li C, Lai L (2021) Dimerization of PHGDH via the catalytic unit is essential for its enzymatic function. J Biol Chem 296:100572
25. Taylor IR, Assimon VA, Kuo SY, Rinaldi S, Li X, Young ZT, Morra G, Green K, Nguyen D, Shao H et al (2020) Tryptophan scanning mutagenesis as a way to mimic the compound-bound state and probe the selectivity of allosteric inhibitors in cells. Chem Sci 11:1892–1904
26. Tabatabaie L, de Koning TJ, Geboers AJ, van den Berg IE, Berger R, Klomp LW (2009) Novel mutations in 3-phosphoglycerate

dehydrogenase (PHGDH) are distributed throughout the protein and result in altered enzyme kinetics. Hum Mutat 30:749–756
27. Vaupel P, Schmidberger H, Mayer A (2019) The Warburg effect: essential part of metabolic reprogramming and central contributor to cancer progression. Int J Radiat Biol 95:912–919
28. Poff A, Koutnik AP, Egan KM, Sahebjam S, D'Agostino D, Kumar NB (2019) Targeting the Warburg effect for cancer treatment: ketogenic diets for management of glioma. Semin Cancer Biol 56:135–148
29. Ngo B, Kim E, Osorio-Vasquez V, Doll S, Bustraan S, Liang RJ, Luengo A, Davidson SM, Ali A, Ferraro GB et al (2020) Limited environmental serine and glycine confer brain metastasis sensitivity to PHGDH inhibition. Cancer Discov 10:1352–1373
30. Maddocks ODK, Athineos D, Cheung EC, Lee P, Zhang T, van den Broek NJF, Mackay GM, Labuschagne CF, Gay D, Kruiswijk F et al (2017) Modulating the therapeutic response of tumours to dietary serine and glycine starvation. Nature 544:372–376
31. He H, Jiang H, Chen Y, Ye J, Wang A, Wang C, Liu Q, Liang G, Deng X, Jiang W et al (2018) Oridonin is a covalent NLRP3 inhibitor with strong anti-inflammasome activity. Nat Commun 9:2550
32. Vasaturo M, Cotugno R, Fiengo L, Vinegoni C, Dal Piaz F, De Tommasi N (2018) The anti-tumor diterpene oridonin is a direct inhibitor of Nucleolin in cancer cells. Sci Rep 8:16735
33. Shen X, Zhao L, Chen P, Gong Y, Liu D, Zhang X, Dai L, Sun Q, Lou J, Jin Z et al (2019) A thiazole-derived oridonin analogue exhibits antitumor activity by directly and allosterically inhibiting STAT3. J Biol Chem 294:17471–17486
34. Yao H, Xie S, Ma X, Liu J, Wu H, Lin A, Yao H, Li D, Xu S, Yang DH et al (2020) Identification of a potent oridonin analogue for treatment of triple-negative breast cancer. J Med Chem 63:8157–8178
35. Raghavendra NM, Pingili D, Kadasi S, Mettu A, Prasad S (2018) Dual or multi-targeting inhibitors: the next generation anticancer agents. Eur J Med Chem 143:1277–1300
36. Ding Y, Ding C, Ye N, Liu Z, Wold EA, Chen H, Wild C, Shen Q, Zhou J (2016) Discovery and development of natural product oridonin-inspired anticancer agents. Eur J Med Chem 122:102–117
37. Thompson JR, Bell JK, Bratt J, Grant GA, Banaszak LJ (2005) Vmax regulation through domain and subunit changes. The active form of phosphoglycerate dehydrogenase. Biochemistry 44:5763–5773
38. Janes MR, Zhang J, Li LS, Hansen R, Peters U, Guo X, Chen Y, Babbar A, Firdaus SJ, Darjania L et al (2018) Targeting KRAS mutant cancers with a covalent G12C-specific inhibitor. Cell 172:578-589 e517
39. Pan S, Jang SY, Liew SS, Fu J, Wang D, Lee JS, Yao SQ (2018) A vinyl sulfone-based fluorogenic probe capable of selective labeling of PHGDH in live mammalian cells. Angew Chem Int Ed Engl 57:579–583
40. Ma P, Xue Y, Coquelle N, Haller JD, Yuwen T, Ayala I, Mikhailovskii O, Willbold D, Colletier JP, Skrynnikov NR et al (2015) Observing the overall rocking motion of a protein in a crystal. Nat Commun 6:8361
41. Yao Z, Xie F, Li M, Liang Z, Xu W, Yang J, Liu C, Li H, Zhou H, Qu LH (2017) Oridonin induces autophagy via inhibition of glucose metabolism in p53-mutated colorectal cancer cells. Cell Death Dis 8:e2633
42. Kwan HY, Yang Z, Fong WF, Hu YM, Yu ZL, Hsiao WL (2013) The anticancer effect of oridonin is mediated by fatty acid synthase suppression in human colorectal cancer cells. J Gastroenterol 48:182–192
43. Huang H, Weng H, Dong B, Zhao P, Zhou H, Qu L (2017) Oridonin triggers chaperon-mediated proteasomal degradation of BCR-ABL in leukemia. Sci Rep 7:41525
44. Mogk A, Bukau B, Kampinga HH (2018) Cellular handling of protein aggregates by disaggregation machines. Mol Cell 69:214–226
45. Sullivan MR, Mattaini KR, Dennstedt EA, Nguyen AA, Sivanand S, Reilly MF, Meeth K, Muir A, Darnell AM, Bosenberg MW et al (2019) Increased serine synthesis provides an advantage for tumors arising in tissues where serine levels are limiting. Cell Metab 29:1410-1421 e1414
46. Reid MA, Allen AE, Liu S, Liberti MV, Liu P, Liu X, Dai Z, Gao X, Wang Q, Liu Y et al (2018) Serine synthesis through PHGDH coordinates nucleotide levels by maintaining central carbon metabolism. Nat Commun 9:5442
47. Ma X, Li B, Liu J, Fu Y, Luo Y (2019) Phosphoglycerate dehydrogenase promotes pancreatic cancer development by interacting with eIF4A1 and eIF4E. J Exp Clin Cancer Res 38:66
48. Zhang W-Z, Tang J-C, Wang S-S, Wang Z-J, Qin W-M, He J-H (2019) The protein complex crystallography beamline (BL19U1) at the Shanghai Synchrotron Radiation Facility. Nucl Sci Tech 30:170
49. Ma J, Chen T, Wu S, Yang C, Bai M, Shu K, Li K, Zhang G, Jin Z, He F et al (2019) iProX: an integrated proteome resource. Nucleic Acids Res 47:D1211–D1217